Dynamic Stability Tests of Spinning Entry Bodies in the Terminal Regime

PETER JAFFE*
Jet Propulsion Laboratory, California Institute of Technology, Pasadena, Calif.

Analytical studies indicate that rolling blunt entry vehicles are susceptible to angle-of-attack divergence in the terminal regime. To investigate this problem, an experimental program was conducted where models were spun up and dropped inside the 500-ft-high Vehicle Assembly Building at Cape Kennedy. The angle-of-attack motion was recorded photographically, and from these data the dynamic stability coefficient was determined. The data confirm the results of the analytic studies and suggest that the dynamic stability coefficient increases, in a favorable way, as the roll rate increases.

Introduction

SIX-degree-of-freedom (6-DOF) computer studies[1] and theoretical analyses[2] have indicated that during the terminal portion of entry, blunt configurations are susceptible to catastrophic total-angle-of-attack (α_t) divergence if they are rolling. The motion is sensitive to the roll rate and the aerodynamic coefficients, particularly the dynamic stability coefficient. Unfortunately, both studies[1,2] are based upon planar concepts, whereas the motion is primarily circular. Substantial uncertainty exists about the appropriateness of using data obtained from planar dynamic stability tests or the correctness of the mathematical dynamic stability model used in the 6-DOF program to predict circular motion. In addition, asymmetric vortex forces, which probably exist in this flight regime, are not considered in the analyses. For these reasons, a test program was conducted in which models were spun up about their axes of symmetry and dropped inside the Vehicle Assembly Building (VAB) at the Kennedy Space Flight Center to obtain free-flight data.

The clear drop area in the VAB is ~470 ft high and more than 60 × 60 ft in cross section. Air currents within the building can be virtually eliminated. Access to the drop platform is quick and easy, and all manner of test support is available in the building. To insure that meaningful information could be obtained, a simulated drop was made numerically with a 6-DOF program for the principal model, a 60° half-angle, blunted cone weighing 4.45 lb and having a base diameter of 14 in. Figure 1 shows predicted time and velocity vs drop distance. The simulated drop took about 8.5 sec. After 3 sec, the model had dropped 110 ft, and the velocity had grown to about 88% of its terminal value of 65 fps. It is during the last 5.5 sec, when the velocity is close to terminal, that the most valuable information is obtained. The α-β motion, assuming a dynamic stability coefficient C_{dyn}† of −0.1 and a roll rate p of 1.27 cps, is shown in Fig. 2. The motion is essentially circular; this simplifies the determination of the α_t history and subsequently C_{dyn}.

Presented as Paper 70-988 at the AIAA Guidance, Control, and Flight Mechanics Conference, Santa Barbara, Calif., August 17–19, 1970; submitted September 2, 1970; revision received February 1, 1971. This paper presents the results of one phase of research carried out at the Jet Propulsion Laboratory, California Institute of Technology, under Contract NAS7-100 sponsored by NASA. The author wishes to acknowledge the efforts of all the people at the Vehicle Assembly Building, Cape Kennedy, who helped with the test and whose combined effort made it possible.

* Member of the Technical Staff, Aerophysics Section. Associate Fellow AIAA.

† The dynamic stability coefficient, $C_{\text{dyn}} = C_{m_q} + C_{m_{\dot{\alpha}}}$ is nominally $\partial C_m/\partial(qd/V) + \partial C_m/\partial(\dot{\alpha}d/V)$.

After considering several alternative methods, the following scheme was settled upon for determining α_t. A small 3-v light was mounted inside the model as far forward from the base as possible, on the axis of symmetry. The original base was replaced by white cardboard with an 8-in.-diam section removed from its center. Viewed from above, a fine point of light appeared against a dark background, which was framed by a white annulus. As α_t increased, the light appeared to move toward the inner edge of the annulus, and α_t was determined from the apparent displacement of the light from the center (Fig. 3).

Test Procedure

The test was conducted at the north end of the transfer area between Bays 3 and 4 in June 1969. The models were dropped from the catwalk of the 250-ton crane which is 466 ft from the floor. A 40 × 40 ft net was suspended 7 ft above the floor to recover the models. All but one of the models landed in the net undamaged. Five configurations were tested: 60° half-angle, sharp and rounded outer-edge blunted cones; and 45°, 51.5°, and 70° half-angle, sharp-edge blunted cones (Fig. 4). Each model was constructed of a 0.50-in.-thick fiberglas shell and a steel ballasting ring which fixed the center-of-gravity (c.g.) location and mass/moment-of-inertia characteristics (see Fig. 3).

During the test a model was mounted on the combination support and spin-up mechanism which grips the model at the

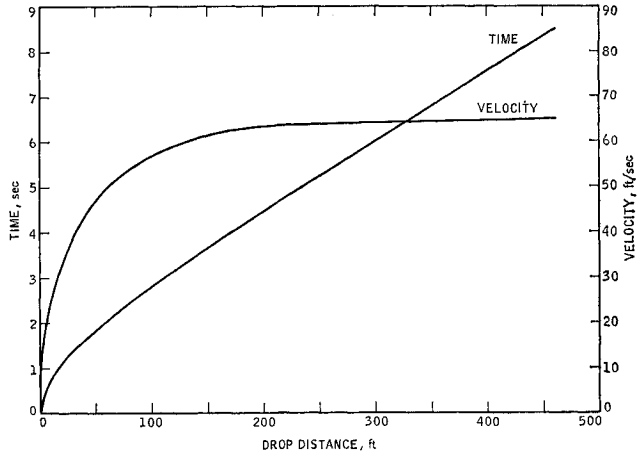

Fig. 1 Predicted time and velocity histories for a typical drop.

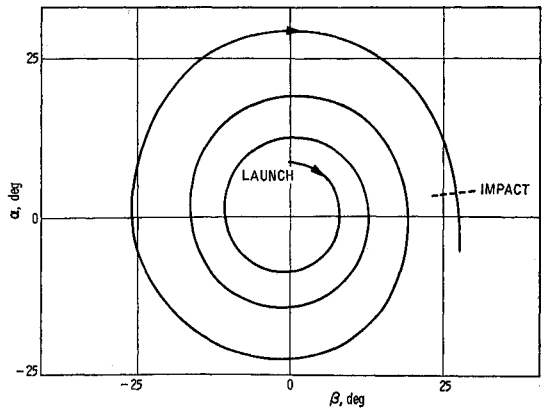

Fig. 2 Predicted alpha-beta motion.

base with three fingers, and a 30-sec countdown was initiated. At −20 sec, the model light was turned on and the model was spun up and placed into position for the drop. Between −5 and −10 sec, the cameras were turned on. At the release time, a light on the floor was turned off. Six 16-mm cameras were used: four with fixed telephoto lenses were clustered around the drop point looking at the base of the model, and two were perpendicular to the drop line, one 154 ft from the floor and the other 356 ft from the floor. The upper cameras nominally ran at 100 frames/sec and the perpendicular cameras operated at 400 frames/sec.

60° Blunted Cone Data

Each of the three models in this group weighed about 4.4 lb, with its center-of-mass ~0.19 diameters aft of the nose. Models 1 and 2 had sharp trailing edges, but the moment-of-inertia of Model 1 was 45% larger than that of Model 2. Model 3 had a rounded trailing edge and about the same moment-of-inertia as Model 1 (see Fig. 4).

Figure 5a contains the α_t reduction for a drop with Model 1 at a roll rate p of 1.30 rps. On the abscissa is the time to reach impact; the model was released (launched) at 8.0 sec and hit the net at zero seconds. The data shown are from three cameras: two Mitchels fitted with 6 and 10-in. focal-length lenses and a Milliken with a 10-in. lens. The three solid curves in Fig. 5a are 6-DOF simulated drops using different effective constant C_{dyn}'s. A C_{dyn} of −0.15 is obviously a good fit of the data; the scatter relative to this curve, at worst, is

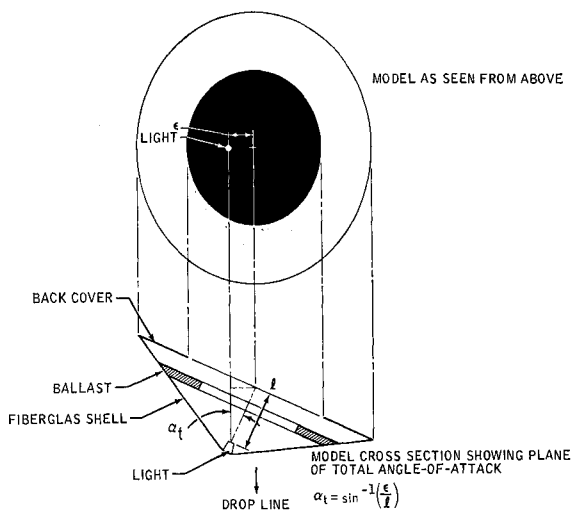

Fig. 3 Model construction and angle-of-attack determination.

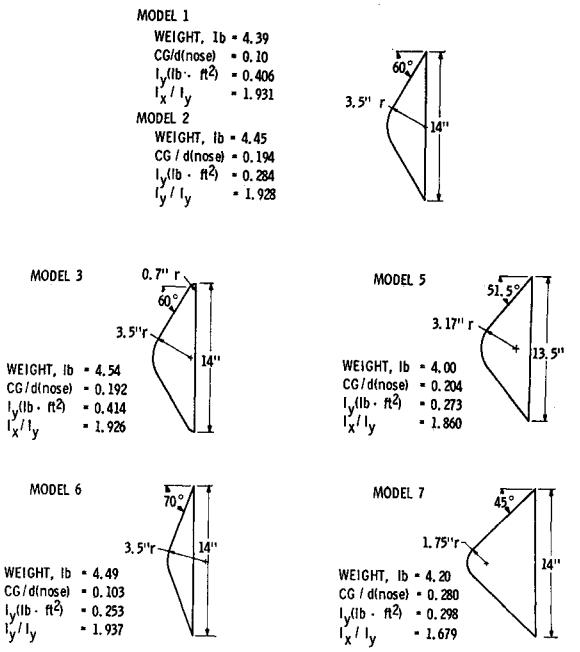

Fig. 4 Model characteristics.

±4°. Figure 5b shows data for the same model at p = 0.65 rps; C_{dyn} is near −0.11. Figures 5c and 5d show data for Model 2 at p = 1.3 and 2.66 rps, respectively; a mean stability coefficient of −0.15 appears to be a good fit for both drops. The data from these four drops, using two different models and three different roll rates, point to a C_{dyn} near −0.15, with a slightly decreasing trend (less negative) at the very low roll rate. This trend is consistent with data from planar tests,[3] which indicate a C_{dyn} of −0.06.

Figures 6a and 6b contain the data for Model 3 (60° blunted cone with rounded trailing edge) at roll rates of 1.30 and 2.61 rps, respectively. A C_{dyn} of −0.10 fits these drops. In addition, we were fortunate in obtaining a good repeat drop at the same conditions as in Fig. 6a. Figure 6c contains the amplitude plot for this run. The (dashed) curve that was faired through the data of Fig. 6a is superimposed on the curve in Fig. 6c but is shifted timewise so that the same amplitude occurs at 4 sec to impact for both drops. The data from the two drops are very consistent, confirming the −0.10 value for C_{dyn} for Model 3.

The somewhat oscillatory nature of the data in Fig. 6a is somewhat puzzling. To discuss it, an appropriate closed-form solution of the α_t motion in this flight regime is introduced. This solution was obtained by specializing the equations developed in Ref. 2 for the case of terminal velocity (i.e., the velocity is constant, and drag is equal to weight):

$$\xi = K_1 e^{-\chi(\zeta-\psi)+i\phi_1' x} + K_2 e^{-\chi(\zeta+\psi)+i\phi_2' x} \qquad (1)$$

where $\chi \equiv x\rho A/4m$; $\zeta \equiv C_{L\alpha} - md^2 C_{dyn}/I$; $\psi \equiv (C_{L\alpha} + md^2 C_{dyn}/I)\, P/(P^2 - 4M)^{1/2}$; and $C_{L\alpha}$, C_D, $C_{m\alpha}$, and $C_{dyn} = C_{mq} + C_{m\dot{\alpha}}$ are the aerodynamic coefficients of lift force slope, drag, pitching moment slope, and dynamic stability; A, d, m, I, I_x are the cross-sectional area, diameter of the body, mass, transverse moment-of-inertia, and longitudinal moment-of-inertia; ρ = air density, V = velocity, x = the distance traveled along the flight path (independent variable), p = roll rate, $P = I_x p/IV$, $M = \rho A d C_{m\alpha}/2I$, and $(\,)'$ denotes derivative operation with respect to x.

The two vector rotational rates, ϕ_1' and ϕ_2', are: $\phi_1' = \frac{1}{2}[P + (P^2 - 4M)^{1/2}]$ and $\phi_2' = \frac{1}{2}[P - (P^2 - 4M)^{1/2}]$. The complex constants K_1 and K_2 are given by the following approximate equations (the subscript "0" denotes the conditions on the onset of terminal velocity): $K_1 \approx (i\xi_0' -$

$\phi_2'\xi_0)/(P^2 - 4M)^{1/2}$ and $K_2 \approx (i\xi_0' + \phi_1'\xi_0)/(P^2 - 4M)^{1/2}$. In addition, there is a trim term K_3 the result of a mass or configurational asymmetry, which rotates at the rate e^{ipt}.

For most of the drops ϕ_1' was 5–30 times larger than ϕ_2', and ξ_0' was relatively small. The motion, therefore, is dominated by the second half of Eq. (1); i.e.,

$$\xi \simeq K_2 e^{-x(\zeta+\psi)+i\phi_2' x} \tag{2}$$

This is the equation of a body rolling at rate p and precessing at a rate $\frac{1}{2}[P - (P^2 - 4M)^{1/2}]$; this type of motion is also predicted by the 6-DOF program.

Applying these equations to drop 16 of Fig. 6a, we obtain $p = 8.3$ rad/sec, $\phi_1' = 0.307$ rad/ft, $\phi_2' = -0.0488$ rad/ft (precession rate), and $\phi_1'/\phi_2' = 6.4$. These values of ϕ_1' and ϕ_2' were computed using the experimental value of p

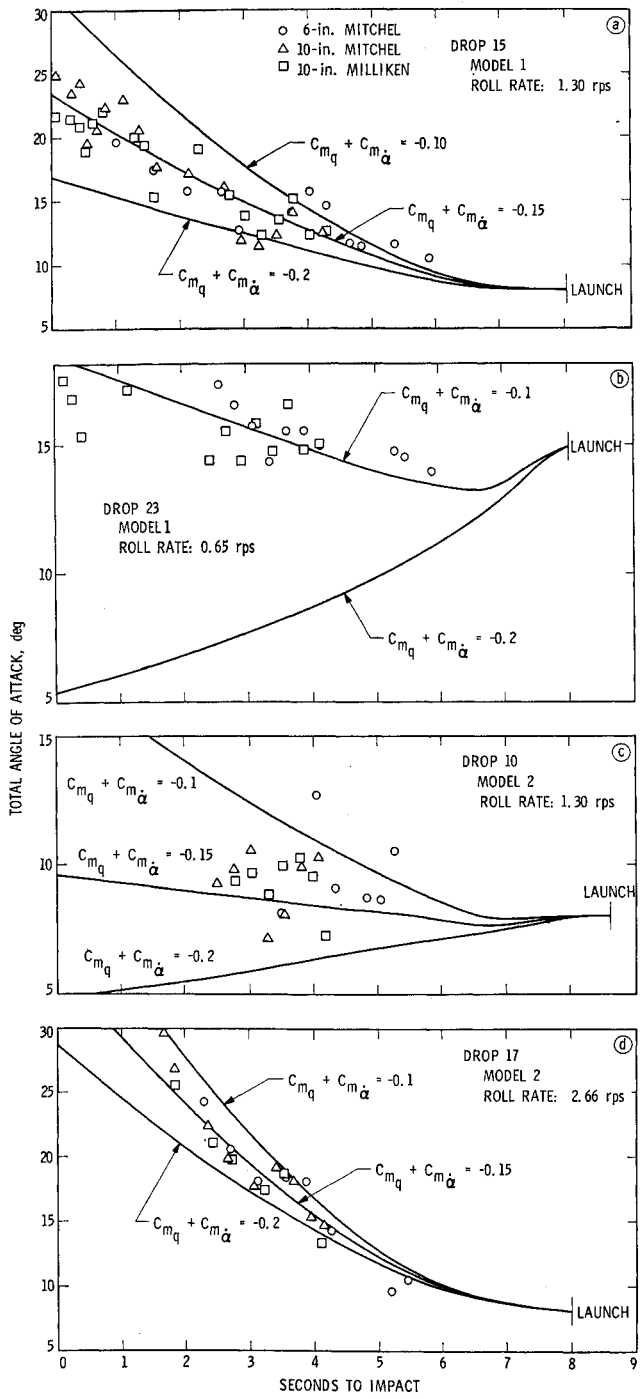

Fig. 5 Reduced data for drops 15, 23, 10, and 17.

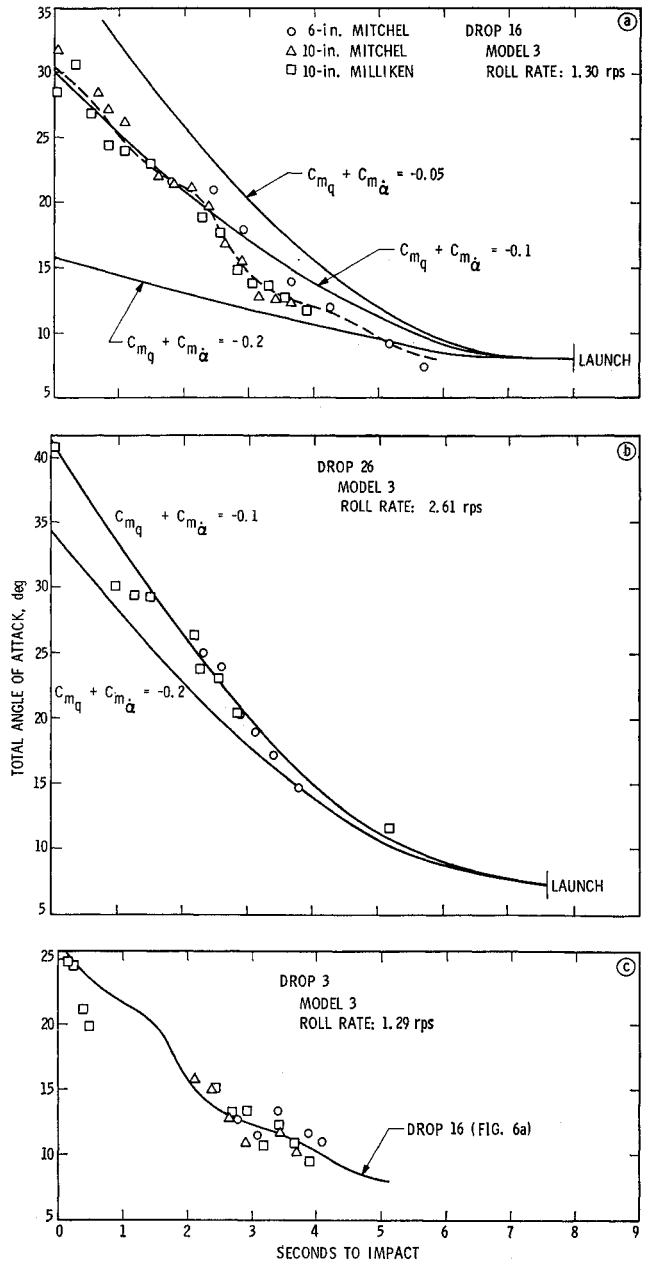

Fig. 6 Reduced data for drops 16, 26, and 3.

but a value of $C_{m\alpha}$ (-0.13) obtained from previously acquired data. In order to verify these numbers, the model precession rate was accurately determined by measuring the rotational motion of the center light with respect to the apparent model center. For drop 16, the measured ϕ_2' was 0.534 rps. To convert the data into rad/ft, the mean velocity was accurately determined from the side cameras; the measured ϕ_2' was -0.0520 rad/ft. The corresponding static stability coefficient, $C_{m\alpha}$, determined from Eq. (2) was -0.14, certainly close to the assumed value of -0.13.

The actual motion and the analytical predicted motion appear to be in good agreement. What then caused the oscillatory perturbations? Several obvious possibilities exist: 1) the K_1 term might not have been negligible, possibly because of an unusually large initial angular velocity; 2) there might have been a trim or what appeared to have been a trim term because the light or annulus was not centered; or 3) the mass of the vehicle might have been distributed asymmetrically, giving rise to cross-products-of-inertia. In regard to the first possibility, the K_1 term rotates at a rate $\phi_1' =$

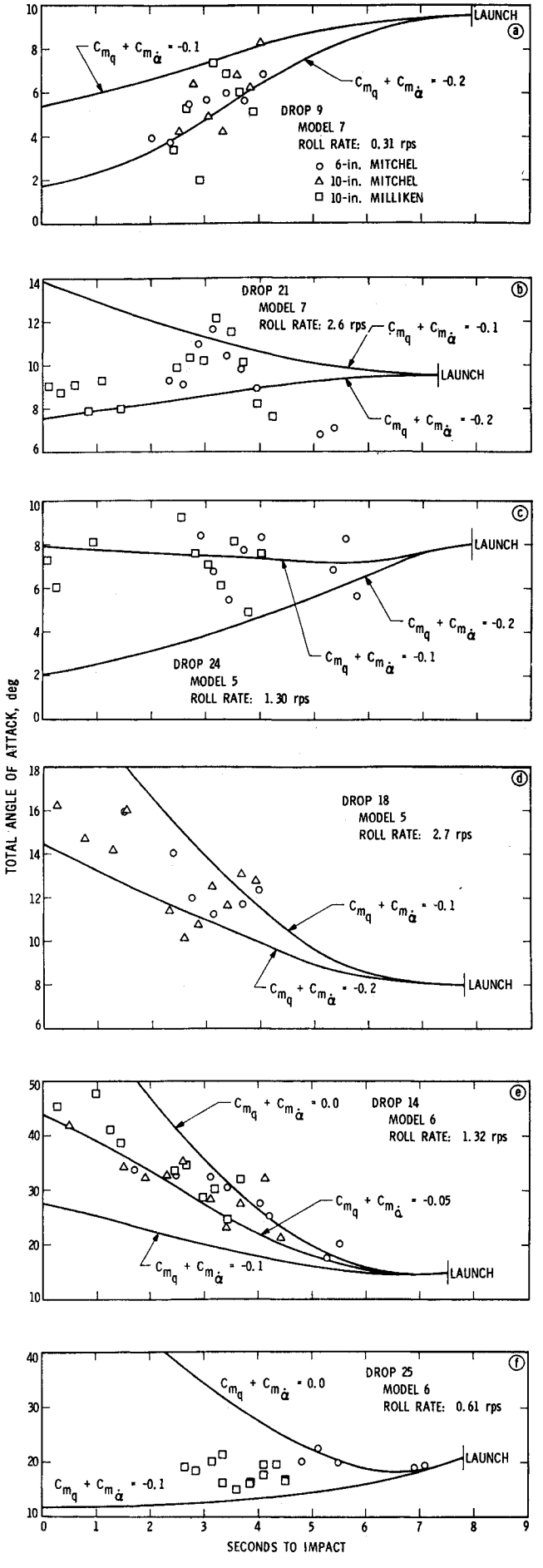

Fig. 7 Reduced data for drops 9, 21, 24, 18, 14, and 25.

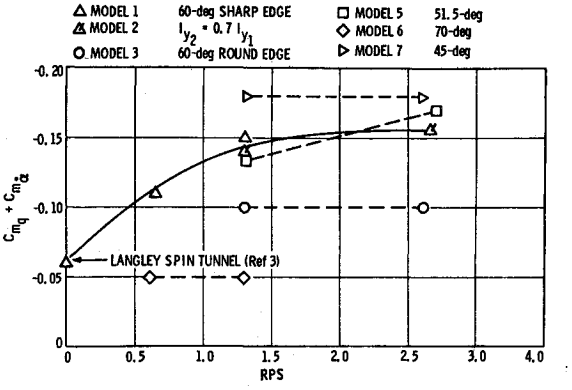

Fig. 8 Summary.

0.307 rad/ft = 3.15 cps, whereas Fig. 6a shows that the oscillatory frequency is only 0.3 cps. The second possibility, a trim term (K_3), also is disqualified because it would rotate at the roll rate, 1.32 rps. Finally, the influences of asymmetric mass distributions were investigated with 6-DOF calculations. Cases of larger than physically probable cross-products-of-inertia, I_{xz} and I_{yz}, and asymmetric transverse moments-of-inertia ($I_y \pm I_z$) were computed. Cross-products-of-inertia produced high frequency but small amplitude ($\sim 1°$) nutations, and the unequal transverse moments-of-inertia cases produced high frequency nutations with even smaller amplitudes.

Six-degree-of-freedom verifications of the influence of initial transverse angular velocities indicated that reasonable values of angular velocity had very little influence on the amplitude motion. They produced perturbations during the early part of the drop which tended to disappear after 3 sec. Large angular velocities did substantially change the amplitude motion by making the K_1 vector dominant but, the values required were physically unrealistic.

The reason for the 0.3 cps oscillatory perturbation remains a mystery. Other possibilities that should be considered are induced flow asymmetries, vortex shedding, and perhaps some transitional phenomena.

45°, 51.5°, and 70° Blunted Cone Data

Figures 7a and 7b contain the results of two drops with the 45° blunted cone at p's of 1.31 and 2.6 rps, respectively. The data appear to lie in a dynamic stability band of -0.1 to -0.2. However, these numbers are questionable, since readings were possible for only 2 sec of the low-p drop (Fig. 7a), and the data from Fig. 7b are very erratic. In comparing these data with data from the 60° blunted cone it must be remembered that the c.g. of this model was farther aft (0.28 diameters, compared to 0.20 diameters). However, since dynamic stability increases as the c.g. is moved forward, and since the experimental values for both configurations were about the same, it is speculated that for the same c.g. position the 45° blunted cone would have been more stable.

The results for the 51.5° blunted cone are included in Figs. 7c and 7d. A C_{dyn} of -0.2 produces a reasonably good simulation for the larger-p drop (Fig. 7d); the lower p (Fig. 7c) appears to favor a somewhat lower C_{dyn}. Unfortunately, the quality of the data is degraded by severe oscillatory perturbations.

Figures 7e and 7f contain the α_t data for 70° blunted-cone drops at p's of 1.32 and 0.61 rps, respectively. The 6-DOF simulations indicate a C_{dyn} of -0.05 or slightly lower. This is less than half the lowest value obtained for any of the other configurations. The two drops demonstrate the extreme sensitivity of this configuration's stability to the roll rate. At 0.61 rps, the vehicle was marginally stable, but at 1.32 rps, it was highly unstable.

Data Summary and Concluding Remarks

The experimental data confirm that blunt entry bodies in the terminal regime experience a substantial decrease in their flight stability when they are rolling. From comparisons between the measured angle-of-attack data and the six-degree-of-freedom simulations, it appears that conventional flight analyses based on a symmetric force model can adequately predict the level of angle-of-attack divergence (or convergence) in this regime. It does not, however, describe or explain the oscillatory perturbations that were observed during most of the drops, and the data are not of high enough quality to accurately describe the perturbations or draw any conclusions about them. With this qualification, the following observations are made from the data summary in Fig. 8: 1) the effective dynamic stability coefficient tends to increase (in a favorable way) as the body roll rate increases; 2) the sharper configurations (smaller cone angles) are more stable than the blunter configurations; and 3) configurations with round trailing edges are slightly less stable than their sharp-edged counterparts.

For anyone contemplating performing similar tests I would suggest that internal instrumentation be considered as an alternative method of obtaining data. The photographic method was convenient and relatively inexpensive, but the quality of the data was not satisfactory for a detailed analysis. Since the models can be recovered undamaged, a gyro-telemetry system might be used.

References

[1] Shirley, D. H. and Misselhorn, J. E., "Instability of High-Drag Planetary Entry Vehicles at Subsonic Speeds," *Journal of Spacecraft and Rockets*, Vol. 5, No. 10, Oct. 1968, pp. 1165–1169.

[2] Jaffe, P., "Terminal Dynamics of Atmospheric Entry Capsules," *AIAA Journal*, Vol. 7, No. 6, June 1969, pp. 1157–1158.

[3] Bendura, R. J., "Low Subsonic Static and Dynamic Stability Characteristics of Two Blunt 120° Cone Configurations," TN D-3853, Feb. 1967, NASA.

JUNE 1971 J. SPACECRAFT VOL. 8, NO. 6

Re-Entry Capsule Dynamics

LARS E. ERICSSON* AND J. PETER REDING†
Lockheed Missiles & Space Company, Sunnyvale, Calif.

A bulbous base can have a profound effect on the aerodynamic characteristics of blunt space capsules and slender re-entry bodies and can cause drastic loss of dynamic stability. A careful examination of available experimental data reveals that the often complex effects of bulbous bases can be explained using quasi-steady separated flow concepts. In general, a bulbous base adversely affects the vehicle dynamics but increases the static stability.

Nomenclature

A_F = forebody axial force, kg; coefficient $C_{AF} = A_F/q_0S$
c = reference length, m (usually $c = d$)
d = body caliber, m
M = Mach number
M_A = axial force pitching moment, kg-m; coefficient, $C_{m_A} = M_A/q_0Sc$
N = normal force, kg; coefficient $C_N = N/q_0S$
q = pitch rate, rad/sec; $q = \dot{\theta}$
q_0 = freestream dynamic pressure, $\rho U^2/2$
R_c = Reynolds number, based on c
S = reference area, m^2, $S = \pi c^2/4$
T = period of oscillation, sec
$t, \Delta t$ = time, sec
U = freestream velocity, m/sec
$\bar{U}$ = mean convection velocity, m/sec
x = horizontal coordinate, m
$\bar{x}$ = x coordinate of body c.g. or oscillation center
ξ = dimensionless x coordinate from body c.g., $\xi = (x - \bar{x})/c$
z = vertical coordinate, m
α = angle-of-attack, rad or deg; α_0 = trim value
$\tilde{\alpha}$ = local cross-flow angle, rad or deg, Eq. (7)
$\bar{\alpha}$ = angle-of-attack envelope, rad or deg
ρ = air density, kg-sec^2/m^4
ω = oscillation frequency, rad/sec; $\bar{\omega} = \omega c/U$
θ = body attitude perturbation, rad or deg

Subscripts

a, s = attached- and separated-flow, respectively
N = nose
0 = initial or unperturbed value

Superscript

i = induced, e.g., $\Delta^i C_N$ = separation-induced normal force coefficient

Differential symbols

$\dot{\theta}(t)$ = $\partial\theta/\partial t$; $\ddot{\theta}(t) = \partial^2\theta/\partial t^2$; $C_{N\alpha} = \partial C_N/\partial\alpha$; $C_{m_\theta} = (\partial C_m/\partial\theta)_{\theta=0}$; $C_{m_q} + C_{m_{\dot{\alpha}}} = C_{m_{\dot{\theta}}} = [\partial C_m/\partial(c\dot{\theta}/U)]_{\theta=0}$; $C_{m_{\dot{q}}} = [\partial C_m/\partial(c\dot{q}/U^2)]_{\theta=0}$

Integrated quantities

$C_{\bar{m}_\theta}$; $C_{\bar{m}_{\dot{\theta}}}$ = defined in Eqs. (18) and (17), respectively

Presented as Paper 70-563 at the AIAA Atmospheric Flight Mechanics Conference, Tullahoma, Tenn., May 13–15, 1970; submitted June 16, 1970; revision received January 13, 1971. The flow concepts used in the paper were developed in studies for NASA under Contracts NAS 8-5338, NAS 8-11238, and NAS 1-6450.

* Senior Staff Engineer. Associate Fellow AIAA.
† Research Specialist. Member AIAA.

Introduction

BULBOUS bases are rather common on modern re-entry vehicles. Manned re-entry capsules usually comprise a blunt heat shield in the wake of which the valuable payload is shielded and supposedly hidden from a hostile environment. On the more slender re-entry configurations used for military applications, convex rounded bases are used for other equally compelling reasons. Although the bulbous base in some cases may have little effect on the static characteristics, it can have drastic effects on the vehicle dynamics, causing un-